CrystEngComm

Accepted Manuscript

ROYAL SOCIETY OF CHEMISTRY

www.rsc.org/crystengcomm

Synthesis, microstructure, growth mechanism and photoluminescence of high quality [0001]-Oriented InN nanowires and nanonecklaces

Huiqiang Liu[a,b]*, Sheng Chu*[a*]*, Rufang Peng*[b*]*, Min Liu*[b]*, Zuxin Chen*[a]*, Bo Jin*[b]*, and Shijin Chu*[b]

a. State Key Laboratory of Optoelectronic Materials and Technology, Sun Yat-Sen University, Guangdong Guangzhou 510275, China

b. State Key Laboratory Cultivation Base for Nonmetal Composites and Functional Materials, Southwest University of Science and Technology, Sichuan Mianyang 621010, China

**Corresponding author: Sheng Chu, Tel: +86-20-84110402, E-mail address: chusheng@mail.sysu.edu.cn;*
Rufang Peng, Tel: +86-816-6089399, E-mail address: pengrufang@swust.edu.cn.

Abstract: Novel indium nitride (InN) based nanomaterial is important for high speed electronics and infrared optoelectronics. In this paper, high quality Indium nitride (InN) nanostructures including nanowires and nanonecklaces, have been grown on one substrate by chemical vapor deposition. The morphologies and microstructures of InN nanowires and nanonecklaces were characterized, which confirmed their chemical composition as well as single crystallinity. The InN nanonecklaces consist of multiple beads composed of two equilateral truncated hexagonal cones faceted with $\left\{10\bar{1}\bar{1}\right\}$ and $\left\{10\bar{1}1\right\}$ planes. The growth mechanism of the InN nanonecklace was studied and a three-step process was suggested for the growth. Finally, room temperature photoluminescence spectra of the two nanostructures showed the near band edge emissions of around 0.73 eV, where the emission from nanonecklace was found to be stronger, indicating the promise for near-infrared optoelectronics applications.

Keywords: InN, CVD, nanonecklaces, nanowires, crystallography, photoluminescence

Introduction

Group III nitride semiconductors are extensively studied materials in the last two decades for broad technologies ranging from light emitters to fast electronics. Among them, much effort was dedicated to the study of InN for its distinguished physical and chemical properties [1-5], especially the high electrical conductivity and electron mobility. These merits may lead to potential applications in high speed electronic devices, terahertz spectroscopy[6], biosensors[7], solar cells[8], high output piezoelectric nanogenerators[9], as well as quantum computing[10], etc.

Recently, like other materials, the interest in nanostructured InN is continuously growing. For example, studies have showed that the diameter and composition along individual InN nanowire can be modulated *in situ* by tuning the seed particle supersaturation via the supply of III and V sources during the growth[11]; quantum confinement in 1 nm wide InN nanowires shifts optical emission to the green/cyan wavelengths and inverts the order of the top valence bands, leading to linearly polarized visible-light emission[12]; C. Yin *et al* found that the spin splitting of the surface electron accumulation layer is effectively tuned as well as spintronic applications via controlled modulation[13]. For the material growth section[14-15], many InN nanostructures, including nanotubes[16], nanorods[17] and nanowires[18-20] have been synthesized by various methods[15–21], such as plasma-assisted molecular-beam epitaxy (MBE), plasma-assisted chemical vapor deposition (CVD), chemical beam epitaxy (CBE), etc. With an in-depth comparison, these methods are all demonstrated to have some limitations. For instance, MBE and CBE grown InN nanorods usually have very limited length and aspect ratios due to slow growth rate; while plasma assisted method requires sophisticated control of N pressure. On the other hand, several reports have shown that furnace CVD method can offer a clean, rapid, and cost effective way to grow InN nanowires/nanorods[22-24]. The versatility of nanomaterials is also important to fully explore their potentials. In this aspect, other forms of nanostructures, such as nanonecklaces, have not been reported in CVD grown InN. In fact, the growth of such peculiar structures is of interest in both fundamental crystallographic studies as well as novel optoelectronic applications. In this study, we have investigated the growth pattern of InN nanowire and nanonecklace via CVD process. It is demonstrated that two kinds of morphologies (nanowires and nanonecklaces) can be grown on one Si substrate simultaneously. The morphology, microstructure, and compositions of these products were systematically characterized. The growth mechanism of InN nanonecklace structure was analyzed and discussed in detail. In such case, a three-step growth mechanism and a tentative growth mode were proposed based on time-dependent growth observation. Furthermore, room temperature photoluminescence (PL) spectra of the two InN nanostructures demonstrated fairly good optical properties, which suggests a wide application potential in nano/microscale optoelectronic devices.

Experimental section

Synthesis and crystal growth

The InN nanostructures were synthesized in a horizontal three-temperature zones tube furnace system. A quartz boat (length 5 cm, height 1 cm) containing 0.4 g of In powder (99.999%, Xiya Reagent) was placed in the middle of the temperature zone 2. An 1.5 cm×1.5 cm silicon (100) substrate coated with a 60 nm gold colloid (BBI Solution) was inversely placed on the top of the quartz boat. In another word, the substrate with gold colloid side faced downward in order to facilitate the growth of InN nanomaterials, and the schematic diagram of tube furnace to synthesize InN nanomaterials is shown in Fig. 1. The quartz tube was degassed to ~2 Pa and then purged with argon (99.999% purity, Messer) and vented to 1 atm. The argon was introduced at one end of the quartz tube at a constant flow rate of 100 sccm (standard cubic centimeters per minute). The temperature zones 1 and 2 of the furnace were simultaneously increased to 700 °C in 30 min, and temperature zone 3 was not particularly heated during the growth. The temperature zone 3 was kept idle, which almost have no impact on the material synthesis. Then the NH_3 (99.99% purity, Messer) was introduced at same end of the quartz tube at a constant flow rate of 250 sccm when the setting temperature was reached. The growth was kept for 80 min. After the reaction the furnace was cooled to room temperature, and gray and black-colored products were found covering the silicon substrate. The N/In ratio was controlled by the NH_3 flow rate while other growth parameters were kept as constant, and the NH_3 flow rate automatic control method based on the mass flow controller (MFC) ranged from 0 sccm to 500 sccm.

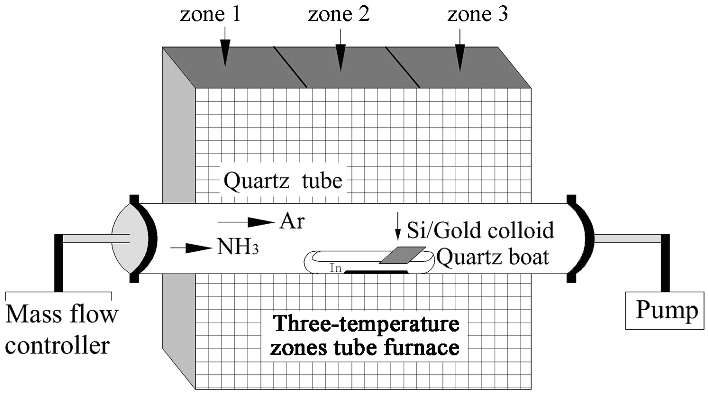

Fig. 1 The schematic diagram of tube furnace to synthesize InN nanomaterials. It should be noted that the Si substrate with gold colloid side faced downward.

Crystal structure and characterization

The morphologies and microstructures of the as-synthesized products were systematically characterized. The X-ray diffraction (XRD) data were obtained with a Philips X'Pert PRO diffractometere equipped with Cu-anode X-ray tube, Ni filter, and the focused optics is obtained with incident beam optics equipped with fixed divergence slit & anti-scatter slit module and hybrid monochromator, 4xGe220 Cu system, respectively. The accelerating voltage was set to 40 kV, with 40 mA flux and measurements were conducted in the 2 theta range of 10-90 deg with a step size of 0.03 deg. The field emission scan electron microscopy (SEM) images were obtained on the Model Uitra 55 from Carl Zeiss, which was equipped with energy dispersive X-ray spectrometer (EDS). The accelerating voltage of SEM was set at 15 kV, and 15 kV for EDS measurements. The transmission electron microscopy (TEM) images were obtained on the Model Libra 200 PE (200kV) from Carl Zeiss. The room temperature spatially resolved PL spectroscopy was carried out on a Model inVia Raman Microscope from RENISHAW Co. UK using a 514 nm from a He-Cd laser as the excitation source and the laser beam is focused down to 10 μm size, and the excitation power is 5 mW.

Results and discussion

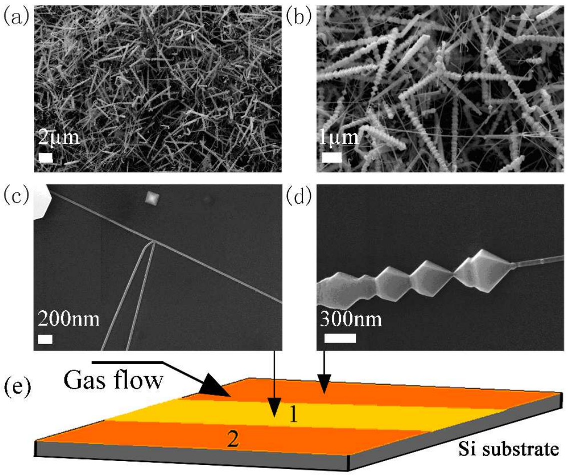

Fig. 2 (a)-(d) SEM images of the nanowire and nanonecklace structures. (e) The schematic diagram of Si (100) substrate to synthesize InN nanomaterials.

The product was first analyzed using SEM (Figs. 2 (a)-(d)). Fig. 2 (a) and (b) are the SEM images of InN nanowires and nanonecklaces, respectively. Magnified SEM images of typical InN nanowire and nanonecklace architecture are shown in Fig. 2 (c) and (d), which exhibit clearly that the typical length and diameter of the individual nanowires range from 5 μm to 10 μm and 30 to 100 nm, respectively. The nanonecklaces consist of varying numbers of connected and uniform beads with up to several micrometers in length; and the major and minor waists range from 90 to 400 and 30 to 150 nm, respectively. The co-existence of different morphologies of nanomaterials suggests that the growth of various nanostructures in CVD may have a wide-range of growth window. Unlike vapor-liquid-solid (VLS) growth mode in Koley *et al*'s report[25], from the SEM (also in subsequent EDS and TEM), the heads or parts of InN nanomaterials in our experiments do not contain gold catalyst, indicating the vapor-solid (VS) growth mode[26]. The role of gold nanoparticles is to increase the surface roughness for nucleation sites to facilitate vapor nucleation. For comparison, we have performed the growth on bare Si substrate, which leaves tiny InN growth, which is not shown here. InN nanostructures could still be obtained, however, in much scarce density, because too clean Si surface brings very few nucleation centers for InN nanostructures growth. Nevertheless, this fact proves that InN nanostructures can be formed without Au, further suggesting VS growth mode. During the growth, variation of local vapor pressures can yield enormously different growth modes. As a matter of fact, we achieved nanonecklace and nanowire growth simultaneously on the same substrate. The positions with nanonecklaces and nanowires coverage are exhibited in Fig. 2 (e), position 1 on Si substrate gets higher In source vapor than position 2. As a result, it can be deduced that In/N source vapor ratio will determine the product morphology. We have performed experiments and confirmed that with fairly small amount of In source, 100% nano-necklaces were achieved (not shown here).

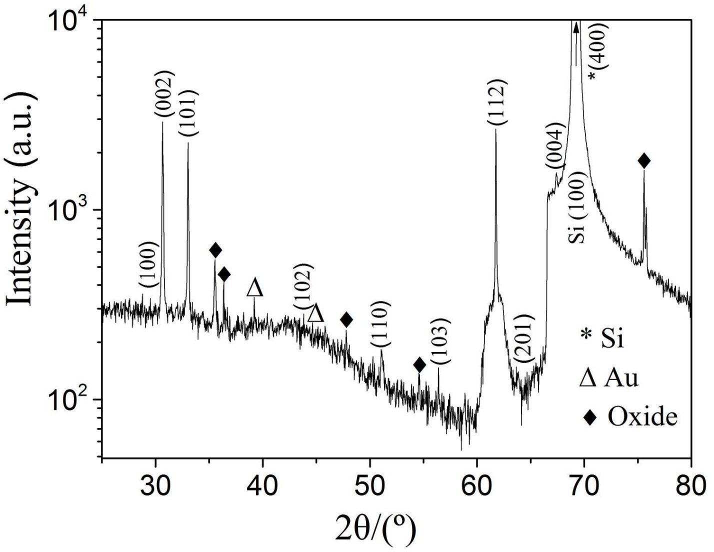

Fig. 3 XRD pattern of the InN nanostructures on Si substrate.

The crystal structure of the as-obtained product was characterized by XRD (Fig. 3). All of the strong reflection peaks can be indexed to wurtzite-type structure InN (w-InN). According to the Bragg equation ($2d\sin\theta = \lambda$) and interplanar spacing formula ($d = \dfrac{a}{\sqrt{\dfrac{4}{3}(h^2 + hk + k^2) + (\dfrac{a}{c})^2 l^2}}$), where d , θ, λ, $\{hkl\}$ are the interplanar spacing, diffraction angle, wavelength, indices of crystal face, respectively. The lattice constants can be calculated as: a=3.533 ± 0.001 Å and c=5.704 ± 0.002 Å (JCPDS card NO. 50-1239), which match well with the (100) and (002) planes of w-InN, respectively, and are also in good agreement with previously reported values[27-28]. EDS measurements were performed to determine the chemical composition of the samples. Fig. 4 (a) illustrates a typical SEM image of sample part that contains both InN nanonecklaces and nanorods, while the EDS spectrum of marked position in Fig. 4 (a) is shown in Figs. 4 (b). Distinct In and N peaks were found to confirm the elemental composition, while the silicon peak originates from the substrate. The atomic ratio of In: N is close to 1:1, suggesting a good stoichiometry of the material. In EDS, it is natural that native SiO_2 on Si surface and other indium related oxides would contribute to the oxygen peak in EDS. Since in the SEM images it is observed that the coverage of InN nanostructures is relatively thin, which results in very strong Si and O related peaks. The C peak is from surface organic absorption/contaminations (for example, lipid in the air) which covered the surface of the sample.

In reports related to InN nanostructures, strong oxygen and carbon peaks are also commonly presented [10,25,29].

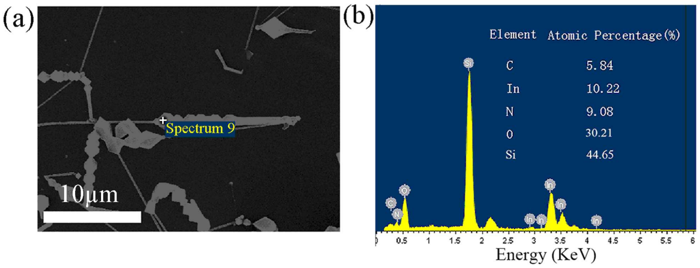

Fig. 4 (a) SEM image of as-synthesized InN nanostructures. (b) The corresponding EDS spectrum of the InN nanostructures taken at spot spectrum 9 marked in (a). Inset: the corresponding composition of the nanostructures determined by EDS.

The microstructures of as-synthesized InN nanostructures were further studied by TEM images of individual InN nanowire and nanonecklace in Figs. 5 (a) and (c), respectively. HR-TEM of Fig. 5 (b) is a magnified presentation of the single nanowire in order to examine detailed crystal structure. The d-spacing of the lattice fringes was measured to be 0.28 nm, matching well with the (0001) plane interspacing of w-InN. The inset of Fig. 5 (b) shows the corresponding selected area electron diffraction (SAED) pattern taken from the nanowire, further confirming that the sample is single-crystalline and grows preferentially along the [0001] crystallographic direction. For the InN nanonecklace sample, Fig. 5 (c) confirms that the nanonecklace consists of multiple connected beads with the major and minor waists ranging from 250 to 400 and 200 to 350 nm, respectively. No grain boundary was found between these beads. HRTEM of Fig. 5 (d) shows fringe with d-spaces of 0.284 nm (also deduced from Fast Fourier transformed (FFT) pattern), in good agreement with the (0001) planes of w-InN. After TEM studies, the crystal structure of the nanonecklaces can be deduced with the assistance of a w-InN unit cell (Fig. 5 (e) right): the growth direction of the nanonecklace is [0001]; the equilateral trapezoid facets of the truncated hexagonal beads are $\left\{10\bar{1}1\right\}$; and the edges between two facets are $\left\langle 2\bar{1}\bar{1}3\right\rangle$. By using the standard lattice parameters of w-InN, the angle between two corresponding facets on the opposite sides of the major waist of the bead (e.g. $\left(10\bar{1}1\right)$ and $\left(10\bar{1}\bar{1}\right)$) is calculated to be 124° and that between two corresponding edges (e.g. $\left[2\bar{1}\bar{1}3\right]$ and $\left[2\bar{1}\bar{1}\bar{3}\right]$) to be 116°. The angle of 117.2° between

$\left[2\bar{1}\bar{1}3\right]$ and $\left[2\bar{1}\bar{1}\bar{3}\right]$ is also in good agreement with the observed values ranging from 116° to 124° in Fig. 5 (c). According to the Wulff construction rule[30], the equilibrium form of crystal would be such as to minimize the total surface energy for a given volume. Thus, the crystal would be bounded by faces located at distances proportional to their surface energies. The largest faces are expected to be the faces with the lowest surface energies. Such faces are also with the greatest interplanar distances d_{hkil}. This fact led to the formulation of the Bravais-Friedel-Donnay-Harker (BFDH) law[31-32] which is used to solve the morphology importance (MI_{hkil}) of the planes. BFDH law determines that the growth rate of the plane (*hkil*) is inversely proportional to the interplanar distance d_{hkil}[33]. In another word, slowest grown plane would be the most stable plane. The BFDH growth rate equation[31,34] is expressed as:

$$\frac{dl_{hkil}}{dt} = \frac{R_{h_1k_1i_1l_1}\sin\gamma + R_{h_2k_2i_2l_2}\sin\alpha - R_{hkil}\sin(\alpha+\gamma)}{\sin\alpha\sin\gamma}$$

Where R_{hkil}, $R_{h_1k_1i_1l_1}$, $R_{h_2k_2i_2l_2}$ are the normal growth rates of the *hkil*, $h_1k_1i_1l_1$, $h_2k_2i_2l_2$ faces, respectively, the growth rate of a given face, such as $\left(10\bar{1}1\right)$ or $\left(10\bar{1}\bar{1}\right)$, is equal to $1/d_{hkil}$ and *t* is the growth time corresponding to the growth of a slice of the crystal with a thickness of the d_{hkil}, the angles γ and α are the appropriate interfacial angles for the given *hkil* plane. From these crystallographic analyses, by using WinX-morph Software[35] on the basis of the above relation, it can be determined that the side facets of InN nanonecklace are $\left\{10\bar{1}\bar{1}\right\}$ planes. The periodic appearing of $\left(10\bar{1}1\right)$ and $\left(10\bar{1}\bar{1}\right)$ finally leads to the formation of corrugated morphology, which is schematically illustrated in Fig. 5 (e). In fact, similar corrugated growth patterns were also observed in 1D wurtzite stacked-cone and zigzag InN[36-37], AlN[38], GaN[39] and ZnO[40] nanostructures.

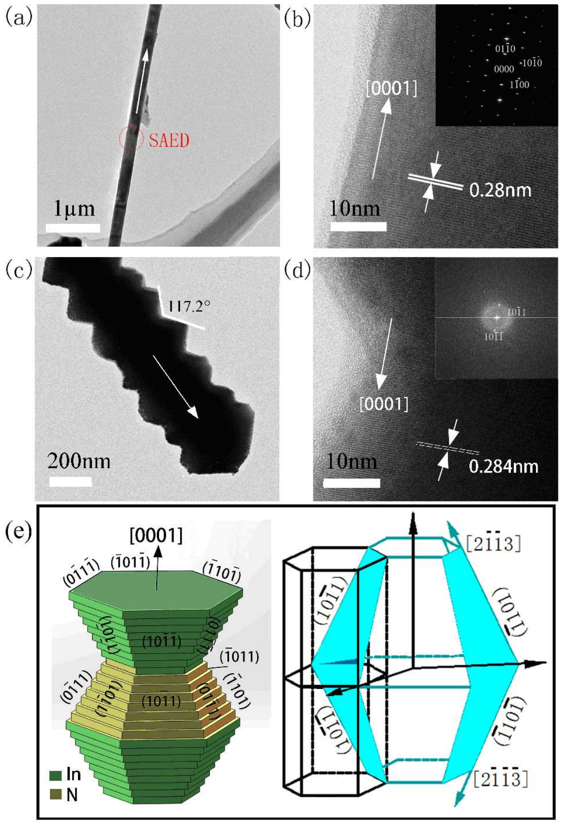

Fig. 5 TEM and HRTEM images of the InN nanowire and InN nanonecklace. (a) TEM image of an individual nanowire, (b) The corresponding HRTEM image and SAED pattern of the nanowire. (c) TEM image of an individual nanonecklace, (d) The corresponding HRTEM image and FFT pattern of the nanonecklace. (e) Space-filling model of ideal [0001] nanonecklace and schematic representation of Miller indexing of the various faces of crystal (left) and the corresponding crystal unit of the InN nanonecklace (right).

Moreover, it should be noted that the above theoretical analysis is based on stoichiometric and ideal slow growth condition. In reality, the growth is also subject to other factors. In the case here, the In/N source ratio would render drastically different growth patterns like nanowires/nanonecklace. This phenomenon is commonly occurred in nanomaterial growth. For example, one CVD growth can yield six different morphologies in Gallium Sulfide structures[41]. Here the detailed theoretical analysis beyond BFDH method is not conducted, since this report is mainly focused on the experiment growth demonstration of peculiar InN nanostructures.

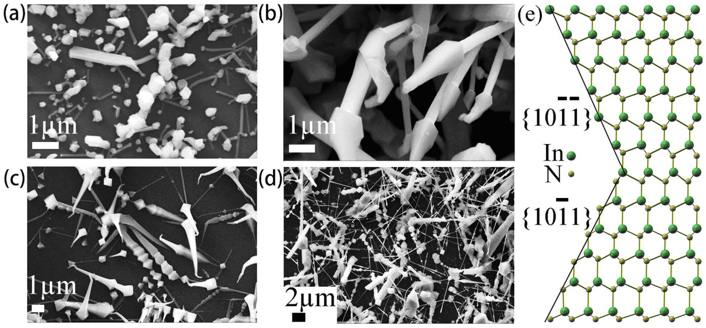

Fig. 6 The SEM images of the entire growth process of InN nanostructures at different growth time under the same growth conditions: (a) Growth time, 10 min. (b) Growth time, 20 min. (c) Growth time, 40 min. (d) Growth time, 60 min. (e) The crystal structure of InN, showing the positively or negatively charged $\{10\bar{1}\bar{1}\}$ and $\{10\bar{1}1\}$ planes.

The growth mechanism of the InN nanonecklaces was investigated in the following part, with emphasis. We synchronously recorded the morphologies of InN architectures at different growth time (10, 20, 40 and 60 min) under the same growth conditions. As shown in Figs. 6 (a)-(d), during the entire growth process of the InN nanostructures, there should apparently exist three steps. The first step is the formation of low density InN nanoparticles on Si surface. During this step, indium atoms and ammonia molecules reacted at high temperatures, and they were gradually deposited on the substrate through the nucleation assisted by gold nucleation sites on the clean Si surface to form the first several layers of w-InN crystal on Si surface (Fig. 6 (a)). It should be noted that all the atoms to form the initial InN layers are stacked in the c-plane of w-InN with a hexagonal shape via a self-assembled process, and the arrival of new In and N atoms can be repeated on previously formed InN layer via homoepitaxial growth[21], as schematically described in Fig. 5 (e). Then, the atom numbers gradually decreased with the deposition of InN from the initial layer to the last one in a truncated hexagonal cone. As a result, the size of (0001) surface gradually decreased and the side facets $\{10\bar{1}\bar{1}\}$ or $\{10\bar{1}1\}$ planes appeared to form the hexagonal cone (Fig. 5(e) and Fig. 6 (a)-(b)) based on the BFDH law[31,34]. Because different terminations of In^{3+}-$\{10\bar{1}\bar{1}\}$ and N^{3-}-$\{10\bar{1}1\}$ planes possess finite charges and dipole moments, they will give a rise to inversely positive and negative electrostatic surface energy. To keep the overall structure stable, the total surface free energy including the electrostatic surface energy and the surface energy should be minimized. When $\{10\bar{1}\bar{1}\}$ (or $\{10\bar{1}1\}$) surface planes crystallize to a certain point, the dipole moment and the electrostatic surface energy continue to increase (the length of dipole and surface area). To minimize the dipole moment and reduce the electrostatic surface energy, the $\{10\bar{1}\bar{1}\}$ (or $\{10\bar{1}1\}$) side facets with an opposite termination will be gradually formed to balance the system energy, as shown in (Fig. 6 (b)-(c)). The alternation of the dipole moments and the change of the electrostatic surface energy will lead to a repeated formation of In^{3+}-$\{10\bar{1}\bar{1}\}$ and N^{3-}-$\{10\bar{1}1\}$ side facets along the c-axis direction and finally producing the InN nanonecklaces with corrugated morphology, as schematically illustrated in Fig. 6 (d). Furthermore, the crystal structure of InN possesses the positively charged In-$(10\bar{1}\bar{1})$ and a negatively charged N-$(10\bar{1}1)$ polar surfaces, resulting in a spontaneous polarization (Fig. 6 (e)). These two surfaces will cause positive and negative electrostatic surface energies. Once $(10\bar{1}\bar{1})$ (or $(10\bar{1}1)$) these two surfaces appears alternately, the overall absolute electrostatic energy can be minimized to close to 0. It is straightforward to show that the first case leads to an increase of surface energy, but a decrease of electrostatic energy. The balance between the surface energy and the electrostatic energy appears to drive the formation of homogeneous InN nanonecklaces. In short, direct synchronous observation of the growth process of the InN nanostructures indicated that three stages were involved: The first several layers of w-InN crystal; formation stages of In-$\{10\bar{1}\bar{1}\}$ and N-$\{10\bar{1}1\}$ side facets; and formation of InN nanonecklaces with corrugated morphology.

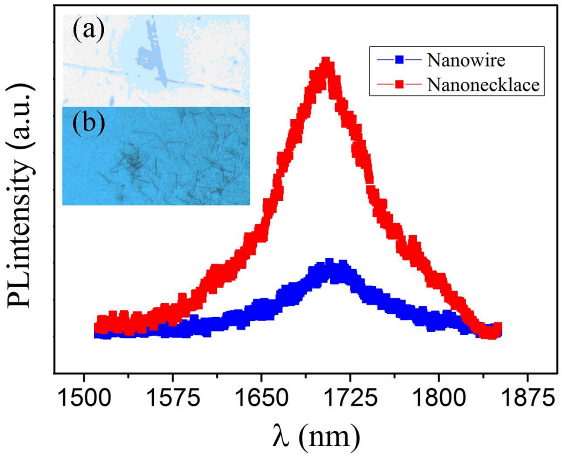

Fig. 7 PL spectra of InN nanostructures at room temperature. The inset shows a magnified image of the InN

nanostructure, (a) nanonecklaces, (b) nanowires.

The PL of the two kinds of structures was investigated (Fig. 7). The strong emission peaks at 0.73 eV can be observed clearly, which is consistent with that measured in n-type degenerate InN. This IR-emission peak position is consistent with the band-to-band emission observed from the high-quality InN nanowires[42-43]. Notefully, the emission intensity from the nanonecklace is stronger, and is tentatively attributed to the larger material size as well as muti-scattering inside one nanonecklace. These high quality InN crystallites have a wide potential application in optoelectronics. For instance, the above InN nanostructures may be used in IR nanocavity lasing, since the size of these crystallites is on the scale of InN emission wavelength[44-45].

Summary

In summary, we have successfully synthesized high quality InN nanowires, and nanonecklaces on one substrate through CVD process. XRD, EDS, and TEM confirmed the synthesis of single crystalline InN nanostructures of wurtzite structure with the growth preferentially along [0001] direction. The nanonecklaces consist of uniform beads composed of two equilateral truncated hexagonal cones faceted with $\left\{10\bar{1}\bar{1}\right\}$ and $\left\{10\bar{1}1\right\}$ planes. Direct synchronous observation of the growth process of the InN nanonecklaces indicated that three stages were involved as shown in the tentative growth model: The first several layers of w-InN crystal; formation stages of In-$\left\{10\bar{1}\bar{1}\right\}$ and N-$\left\{10\bar{1}1\right\}$ side facets; and formation of InN nanonecklaces with corrugated morphology. PL spectra of these InN nanostructures demonstrated the emission peak is around 0.73 eV and the emission intensity from the nanonecklace is stronger. These merits indicate that they could find promising applications in optoelectronic devices.

Acknowledgments

We appreciate financial support from the National Natural Science Foundation of China (grant No. 51372211), youth Innovation Research Team of Sichuan for Carbon Nanomaterials (2011JTD0017), and Chinese Academy of Engineering Physics project CAEPTHZ201302.

References

[1] S. Heedt, C. Morgan, K. Weis, D. E. Bürgler, R. Calarco, H. Hardtdegen, D. Grützmacher, and Th. Schäpers, *Nano Lett.*, 2012, **12**, 4437.

[2] R. X. Yan, D. Gargas and P. D. Yang, *Nat. Photonics*, 2009, **3,** 569.

[3] F. Werner, F. Limbach, M. Carsten, C. Denker, J. Malindretos and A. Rizzi, *Nano Lett.*, 2009, **9,** 1567.

[4] S. Zhao, B. H. Le, D. P. Liu, X. D. Liu, M. G. Kibria, T. Szkopek, H. Guo, and Z. Mi, *Nano Lett.,* 2013, **13**, 5509.

[5] C. Blomers, J. G. Lu, L. Huang, C. Witte, D. Grützmacher, H. Lüth, and Th. Schäpers, *Nano Lett.,* 2012, **12**, 2768.

[6] H. Ahn, C. C. Yu, P. Yu, J. Tang, Y. L. Hong and S. Gwo, *Opt. Express*, 2012, **20**, 769.

[7] Ó. Estebana, F. B. Naranjoa, N. Díaz-Herrerab, S. Valdueza-Felipa, M. C. Navarretec and A. González-Canob, *Sens. Actuators*, 2011, **B158**, 372.

[8] E. C. Garnett, M. L. Brongersma, Y. Cui and M. D. McGehee, *Annu. Rev. Mater. Res.*, 2011, **41**, 269.

[9] C. T. Huang, J. Song, C. M. Tsai, W. Lee, D-H. Lien, Z. Gao, Y. Hao, L. Chen and Z. L. Wang, *Adv. Mater*., 2010, **22**, 4008.

[10] L. B. Huang, D. D. Li, P. C. Chang, S. Chu, H. Bozler, I. S. Beloborodov, and J. G. Lu, *Physics Review B,* 2011, **83**, 245310.

[11] S. K. Lim, S. Crawford, G. Haberfehlner and S. Gradečak, *Nano Lett*., 2013, **13**, 331.

[12] D. Bayerl and E. Kioupakis. *Nano Lett.*, 2014, **14**, 3709.

[13] C. Yin, H. Yuan, X. Wang, S. Liu, S. Zhang, N. Tang, F. Xu, Z. Chen, H. Shimotani, Y. Iwasa, Y. Chen, W. Ge and B. Shen, *Nano Lett*., 2013, **13**, 2024.

[14] J. Zhang, H. Liu, R. Huang, T. Kong, and G. Cheng, *J. Nanoeng. Nanomanuf.*, 2012, **2**, 112.

[15] G Xu, Z. Li, J. Baca, and J. Wu, *Nanoscale. Res. Lett.*, 2010, **5**, 7.

[16] K. Sardar, F. L. Deepak, A. Govindaraj, M. M. Seikh, and C. N. R. Rao, *Small*, 2005, **1**, 91.

[17] N. J. Ku, J. H. Huang, C. H. Wang, H. C. Fang and C. P. Liu, *Nano Lett*., 2012, **12**, 562.

[18] H. D. Espinosa, R. A. Bernal and M. Minary-Jolandan, *Adv. Mater*., 2012, **24**, 4656.

[19] S. H. Park, G. Yuan, D. Chen, K. Xiong, J. Song, B. Leung, and J. Han, *Nano Lett.*, 2014, **14**, 4293.

[20] N. P. Dasgupta, J. Sun, C. Liu, S. Brittman, S. C. Andrews, J. Lim, H. Gao, R. Yan and P. D.Yang, *Adv. Mater*., 2014, **26**, 2137.

[21] P. K. B. Palomaki, E. M. Miller and N. R. Neale, *J. Am. Chem. Soc.*, 2013, **135**, 14142.

[22] M. S. Hu, W. M. Wang, T. T. Chen, L. S. Hong, C. W. Chen, C. C. Chen, Y. F. Chen, K. H. Chen, and L. C. Chen, *Adv. Funct. Mater.*, 2006, **16**, 537.

[23] H. Liu, L. Shi, X. Geng, and S. Xie, *Nanotechnology*, 2010, **21**, 245601.

[24] P. Yang, R. Yan and M. Fardy, *Nano Lett.*, 2010, **10**, 1529.

[25] G. Koley, Z. Cai, E. B. Quddus,J. Liu, M. Qazi, and R. A Webb, *Nanotechnology*, 2011, **22**, 295701.

[26] P. Sahoo, S. Dhara, S. Amirthapandian, M. Kamruddin, S. Dash, B. K.Panigrahi and A. K. Tyagi, *Cryst. Growth. Des.*, 2012, **12**, 2375.

[27] K. M. Yu, Z. Liliental-Weber, W. Walukiewicz, W. Shan, J. W. Ager III, S. X. Li, R. E. Jones, E. E. Haller, Hai Lu, and William J. Schaff, *Appl. Phys. Lett.,* 2005, **86**, 071910.

[28] M. Tangi, J. Kuyyalil, and S. M. Shivaprasad, *J. Appl. Phys.,* 2012, **112**, 073510.

[29] Z. Cai, S, Garzon, M. V. S. Chandrashekhar, R.A. Webb, and G. Koley, *J. Electron. Mater.,* 2008, **37**, 585.

[30] G. Wulff, *Z. Kristallogr*, 1901, **34**, 449.

[31] J. D. H. Donnay, D. Harker, *Am. Mineral*, 1937, **22**, 446.

[32] J. Prywer, *J. Cryst. Growth*, 2004, **270**, 699.

[33] M. A. Deij, J. van Eupena, H. Meekes, P. Verwer, P. Bennemab, and E. Vlieg, *Int. J. Pharm.,* 2008, **353**, 113.

[34] H. Yadav, N. Sinha, B. Kumar, *CrystEngComm*, 2014, **16**, 10700.

[35] W. Kaminsky, *J. Appl. Crystallogr.,* 2005, **38**, 566.

[36] X. Ji, S. Cheng, H. Hu, H. Li, Z. Wu and P. Yan, *AIP ADVANCES*, 2012, **2**, 022150.

[37] H. Liu, S. Xie, and G. Cheng, *CrystEngComm*, 2011, **13**, 3649.

[38] H. Wang, Z. Xie, Y. Wang, W. Yang, Q. Zeng, F. Xing, and L. An, *Nanotechnology,* 2009, **20**, 025611.

[39] F. Yuan, B. Liu, Z. Wang, B. Yang, Y. Yin, B. Dierre, T. Sekiguchi, G. Zhang and X. Jiang, *ACS Appl. Mater. Interfaces,* 2013, **5**, 12066.

[40] A. M. Glushenkov, H. Zhang, J. Zou, G. Q. Lu and Y. Chen, *J. Cryst. Growth,* 2008, **310**, 3139.

[41] G. Z. Shen, D. Chen, P. C. Chen, and C. Zhou, *ACS nano.,* 2009, **3**, 1115.

[42] S. Vaddiraju, A. Mohite, A. Chin, M. Meyyappan, G. Sumanasekera, B. W. Alphenaar, and M. K. Sunkara, *Nano Lett.*, 2005, **5**, 1625.

[43] M. C. Johnson, C. J. Lee, E. D. Bourret-Courchesne, S. L. Konsek, S. Aloni, W. Q. Han, and A. Zettl, *Appl. Phys. Lett.,* 2004, **85**, 5670.

[44] S. Juen, K. Uberbacher, J. Baldauf, K. F. Lamprecht and R. A. Hopfel, *Appl. Phys. Lett.*, 1993, **62**, 1958.

[45] A. Zubrilov, M. E. Levinshtein, S. L. Rumyantsev and M. S. Shur, *John Wiley & Sons, Inc. New York*, 2001, 49.